Modal phase matching in nanostructured zinc-blende semiconductors for second-order nonlinear optical interactions

Eleonora De Luca,[1,*] Reza Sanatinia,[1,†] Mounir Mensi,[2] Srinivasan Anand,[1] and Marcin Swillo[1,‡]

[1]*School of Engineering Sciences (SCI), KTH Royal Institute of Technology, Roslagstullsbacken 21, SE-10691 Stockholm, Sweden*

[2]*School of Engineering Sciences (SCI), KTH Royal Institute of Technology, Electrum 229, SE-16440 Kista, Sweden*

(Received 19 May 2017; revised manuscript received 3 July 2017; published 7 August 2017)

We demonstrate enhanced second-harmonic generation in arrays of nanowaveguides satisfying modal-phase-matching condition, both theoretically and experimentally. The overlap of interacting fields defined by the fundamental mode of the pump and the second-order mode of the second-harmonic wave is enhanced by the longitudinal component of the nonlinear polarization density. For guided modes with significant longitudinal electric field components, the overlap of fields is comparable to that obtained in the quasi-phase-matching technique leading to higher conversion efficiencies. Thus, the presented method is preferable to achieve higher conversion efficiency in second-order nonlinear processes in nanowaveguides.

DOI: 10.1103/PhysRevB.96.075303

I. INTRODUCTION

Second-harmonic generation (SHG) is used in a variety of applications, including generation of visible coherent light sources [1], probing quality of the surfaces [2–4], quantum communication [5], identification of crystal structure [6–8], biosensing [9,10], imaging in scattering media [11] or biological elements [12,13], and nonlinear microscopy [13–15].

Aside from having a large $\chi^{(2)}$, many semiconductors offer a powerful technological platform, supporting the integration of photonic circuits [16,17]. Many III-V compounds, such as gallium phosphide [3,18–21], gallium arsenide [22–25,25–31], and aluminum gallium arsenide [25–28,30,32–35], fall into this category.

Among different III-V compounds, zinc-blende gallium phosphide (GaP), which belongs to the $-43m$ space group, shows remarkable optical properties: large refractive index [36], large second-order nonlinear coefficient [37], large thermal conductivity [38], and broad transparency range [36], which make this material an excellent candidate for nonlinear optical applications.

Although $-43m$ semiconductors lack birefringence, efficient SHG can be achieved by satisfying momentum conservation of optical waves, by using modal phase matching (MPM) or quasi-phase matching (QPM). QPM can be obtained by periodic modulation of the nonlinear coefficient [18,26,27,32,39], but difficulties in the fabrication limit the present applications of GaP [18].

MPM, instead, is based on modal dispersion engineering of different interacting optical modes in the nonlinear process [25,29,33,34]. MPM can be fulfilled by propagating the SHG light in a higher-order mode than the one used for the fundamental wave. However, this requires an excellent overlap of the interacting fields.

One important requirement for presented MPM method in zinc-blende material is the possibility to confine the pump light in TM-like mode. In this respect, nanopillars (NPs) and slab waveguides (SWs) fabricated in a semiconductor (due to high refractive index contrast) would be ideal structures to study MPM.

In this work, we study theoretically and experimentally MPM in arrays of GaP nanopillars and slab nanowaveguides. Compared to individual nanopillars and slab waveguides, their arrays offer two main advantages: (1) they permit less constraint on fabrication, i.e., they allow larger dimensions as well as more tolerant fabrications, and (2) they can be used in metasurfaces for beam manipulation [40–42], e.g., nonlinear beam shaping.

In this paper, we show that in arrays of nanopillars or of slab waveguides, it is possible to obtain an efficient SHG conversion using simultaneously two elements of the nonlinear susceptibility tensor for a wide wavelength range. Moreover, we compare analytically the efficiency of phase-matched SHG in MPM with respect to the case of QPM, where we consider an example structure of a single-slab waveguide.

In addition to the possibility of achieving phase matching in arrays of nanopillars or slab waveguides, their geometries, polarization properties, and dispersion make these nanostructures interesting to be used as nanoscopic light sources, nonlinear beam shaping, and as light conversion components in integrated photonic circuits.

II. ANALYSIS OF SECOND-ORDER OPTICAL NONLINEARITY IN NANOWAVEGUIDES IN ZINC-BLENDE CRYSTALS

For the crystal symmetry $-43m$ (zinc-blende), the only nonvanishing nonlinear coefficients in the bulk crystal are $d_{14} = d_{25} = d_{36} = d$ [43].

For the coordinate system [Fig. 1(a)], i.e., 45° rotated with respect to the crystallographic axes of the crystal, the coefficients d_{14} and d_{36} define the following components of the second-order nonlinear polarization density $\mathbf{P}^{(2)}$:

$$P_x^{(2)} = 2\varepsilon_0 d_{14} E_x E_z e^{(-i2\beta_0 z)}, \tag{1}$$

$$P_z^{(2)} = \varepsilon_0 d_{36} E_x^2 e^{(-i2\beta_0 z)}, \tag{2}$$

*eldl@kth.se

†Present address: School of Engineering and Applied Sciences, Harvard University, Cambridge, Massachusetts 02138, USA.

‡marcin@kth.se

 ©2017 American Physical Society

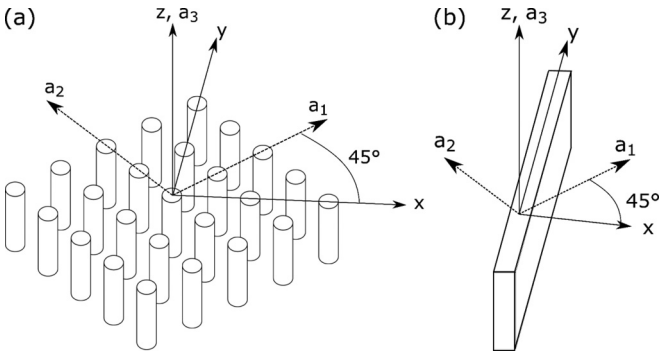

FIG. 1. Orientation of the nanowaveguides with respect to the crystallographic axes ($\mathbf{a}_1$, $\mathbf{a}_2$, $\mathbf{a}_3$) in a zinc-blende crystal. (a) Array of nanopillars. (b) Single-slab waveguide.

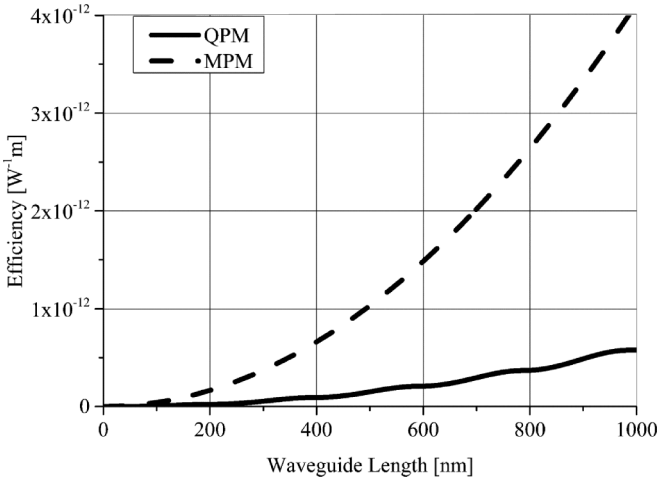

FIG. 2. Efficiency of SHG process for continuous wave pump at the wavelength of 1.2 μm in a single-slab waveguide with a core thickness of 180 nm. The dashed line represents the efficiency obtained through the modal-phase-matching method, while the solid line represents the implementation of the quasi-phase-matching method.

where β_0 is the propagation constant of the guided mode for the fundamental frequency and E_x, E_y, E_z are the corresponding electric field components. For a GaP cylindrical nanowaveguide with air cladding, the strong confinement of guided pump in the fundamental mode HE_{11} can lead to comparable amplitudes of the transverse and the longitudinal components of the electric field. In that case, generated $P_x^{(2)}$ has the largest value and can have good overlap with the second-order mode of the second-harmonic frequency [20]. This configuration can be applied for the array of cylindrical nanowaveguides, where the E_x component of the pump in HE_{11} mode has larger extinction ratio than E_y. The symmetry of $P_x^{(2)}$ and $P_z^{(2)}$ distribution in the X-Y plane allows both of them to excite the same TM_{01} mode and, in addition, $P_x^{(2)}$ can excite HE_{21} mode. If the PM condition is satisfied, all of the three processes can take place simultaneously, enhancing the conversion efficiency.

The amplitude of the mode excited by polarization $\mathbf{P}$ can be calculated in the same way as presented in [44]. By applying nondepleted pump approximation the amplitude of TM_{01} and HE_{21} modes (A_1 and A_2, respectively) can be calculated by using the following equations:

$$\frac{dA_1}{dz} = -i2\omega_0 \iint dx\,dy\left(P_x^{(2)}E_{x,1}^* + P_z^{(2)}E_{z,1}^*\right)e^{i(\beta_1-2\beta_0)z} \tag{3}$$

and

$$\frac{dA_2}{dz} = -i2\omega_0 \iint dx\,dy\left(P_x^{(2)}E_{x,2}^*\right)e^{i(\beta_2-2\beta_0)z}, \tag{4}$$

where the indices 1 and 2 of the electric field profiles refer to the normalized TM_{01} and HE_{21} modes, respectively, with β_1 and β_2 as corresponding propagation constants. Substituting $P_x^{(2)}$ and $P_z^{(2)}$ from Eqs. (1) and (2) into Eqs. (3) and (4), the electric field profiles at the end of the nanowaveguide array can be expressed as

$$E_x^{(2)} = A_1(L)E_{x,1}e^{(-i\beta_1 L)} + A_2(L)E_{x,2}e^{(-i\beta_2 L)} \tag{5}$$

and

$$E_y^{(2)} = A_1(L)E_{y,1}e^{(-i\beta_1 L)} + A_2(L)E_{y,2}e^{(-i\beta_2 L)}, \tag{6}$$

where L is the length of the nanowaveguide.

As one can see, the SHG process depends on the field overlap defined by the integrals in Eqs. (3) and (4) as well as on the relative phase between individual fields. The contribution of $P_z^{(2)}$ to the field overlap with TM_{01} mode results in an enhancement of the SHG process. On the other hand, the phase mismatch caused by the difference between β_1 and $2\beta_0$, as well as between β_2 and $2\beta_0$, reduces the total SHG intensity. Furthermore, the polarization of SHG light is determined by the excitation and phase difference between modes $TM_{01}(\beta_1)$ and $HE_{21}(\beta_2)$.

In order to compare the MPM technique with the QPM method, we considered a single-slab waveguide with air cladding in the same coordinate system (rotated 45°) as in Fig. 1(b). For the MPM case, we assumed the waveguide in $(1\bar{1}0)$ plane with the light propagation in the z direction. Then, the pump guided in TM_0 mode ($E_x^{(\omega)}$, $E_z^{(\omega)}$) excites the SHG light in the TM_1 mode ($E_x^{(2\omega)}$, $E_z^{(2\omega)}$), so that the polarization of the generated light is the same as for the pump. This is a similar case of the example presented above and shows the relation between QPM and MPM techniques. In the QPM method, on the other hand, we consider the slab waveguide in (001) plane, due to the fabrication process consisting mainly in the growth of the different domains [19,22]. Here, the light propagation is in the y direction. Then, the pump guided in TE_0 mode ($E_x^{(\omega)}$) excites the SHG light in the TM_0 mode ($E_y^{(2\omega)}$, $E_z^{(2\omega)}$). The momentum mismatch between the two interacting modes is compensated by the Bloch wave vector $\mathbf{K}_G = 2\pi/\Lambda$.

For the QPM case, we assumed that the waveguide is fabricated with the orientation-patterned growth of GaP and, therefore, $\Lambda = 0.4$ μm corresponds to the period of alternating sign of the nonlinear coefficient.

The simulation results of SHG light intensity for a continuous wave pump with a wavelength of 1.2 μm and a slab width of 180 nm are presented in Fig. 2. The conversion efficiency presented in Fig. 2 is normalized to the power density of the guided pump. Since the guided modes are not confined in

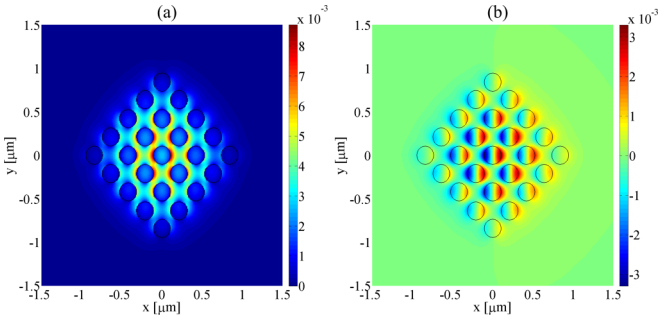

FIG. 3. E_x (a) and E_z (b) electric field profiles of the mode HE_{11} in a GaP array of 5 × 5 nanopillars for the wavelength of 1140 nm (pump).

one of the transverse directions to the light propagation in infinitely wide slab, the power density is defined as a power of the guided light per unit width of the waveguide. The higher efficiency obtained by the MPM method with respect to QPM is due to both the use of modal dispersion and the longitudinal nonlinear polarization density $P_z^{(2)}$, which make the total field overlap value [Eq. (3)] similar to the QPM case. Therefore, MPM is preferable for second-order nonlinear processes in nanowaveguides with significant longitudinal electric field component.

III. ANALYSIS OF THE MODAL DISPERSION AND THE FIELD PROFILES

As previously stated, there are two important features to achieve an efficient SHG on which we concentrated our attention: (1) the fulfillment of PM condition, and (2) the overlap of the modes interacting in the SHG process. We limited our simulations to wavelengths ranging from 1020 to 1220 nm.

The simulations made for the NPs array were performed using a finite element method simulator (COMSOL MULTIPHYSICS 5.0). Through these simulations, the effective refractive indices and the different field profiles interacting in the wave-mixing process were determined. The NPs array analyzed consists of a square lattice of 5 × 5 NPs, with the diameter of 220 nm and the height of 750 nm, the pitch of the array is 300 nm. Diameter and pitch were assumed as constant along the whole height, limiting the analysis of the field profile to a two-dimensional model. The calculated electric field profiles of E_x and E_z are shown in Fig. 3. These, corresponding to the fundamental guided mode (HE_{11}) for $\lambda = 1140$ nm, are the dominant electric field components for the pumping mode. From this analysis, two modes of the calculated SHG wavelengths have the largest contribution: HE_{21} and TM_{01}, presented in Fig. 4.

Since HE_{21} and TM_{01} played the most important role in the satisfaction of PM condition, in Fig. 5 it is shown the calculated effective refractive indices of three modes: the fundamental mode HE_{11} of the pump and two second-order modes for SHG wavelength, HE_{21} and TM_{01}. The normalized intensity (Fig. 5) of the SHG light has been calculated considering the dispersion of all the modes presented in Fig. 5, assuming that the nonlinear coefficient d is wavelength independent and the normalization of the field profiles, as presented in [44], is applied for all

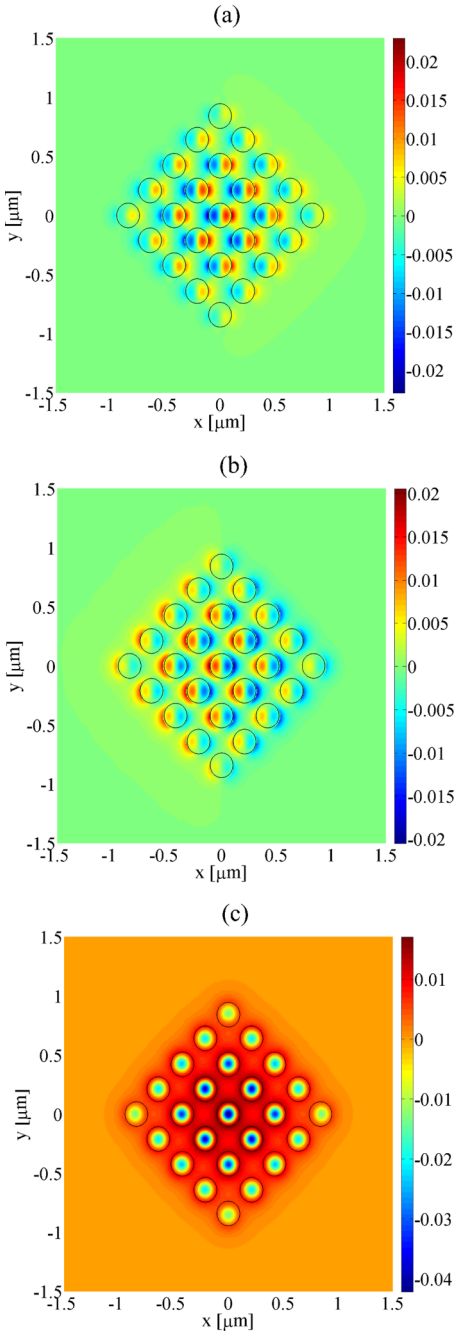

FIG. 4. Electric field profiles of the modes excited in the SHG process at 570 nm in a GaP array of 5 × 5 nanopillars. (a) E_x field for the mode HE_{21}. (b) E_x field for the mode TM_{01}. (c) E_z field for the mode TM_{01}.

the field components. The value of the nonlinear coefficient is $d = 70$ pm/V at 1064 nm wavelength [37]. Since the value of d does not change significantly in the considered wavelength range of the pump [45], the value was kept constant for all the simulations.

We used a similar approach to the one presented for NPs in the case of SWs array. A numerical solution of the transfer matrix method has been used to calculate the electric field profiles and the effective refractive indices.

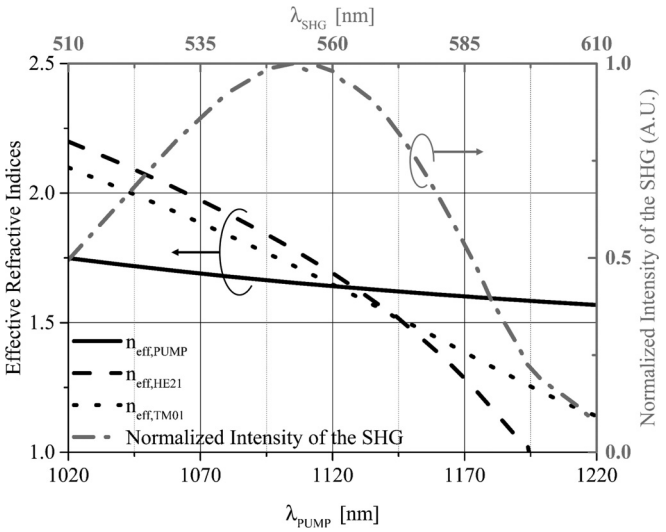

FIG. 5. Normalized SHG intensity (I_x) for an array of 5 × 5 GaP nanopillars (dashed-dotted line) and the effective refractive index of interacting modes in SHG process: HE_{11} for the pump wavelength (solid line), HE_{21} and TM_{01} for the SHG wavelength (dashed and dotted line, respectively).

In this case, the modes interacting in the process are TM_0 (pump) and TM_1 (SHG). In Figs. 6 and 7 the E_x and E_z fields profiles of the pump and the SHG are shown, respectively. The simulated nanostructure consists of five slabs with 205 nm width and 750 nm height; around each slab there is an air gap of 60 nm. In Fig. 8, the dispersion is presented for the mode TM_0 at the pump wavelength and the mode TM_1 at the SHG wavelengths. In the same figure, it is possible to see the evolution of the normalized intensity as a function of the wavelength. When comparing Figs. 5 and 8, one can see a larger bandwidth of SHG in SWs array. This can be explained by a smaller dispersion between effective refractive indices (for the modes guiding SHG light and the pump) in case of SWs array. Also, in both graphs it is visible that the wavelength corresponding to the maximum SHG intensity is

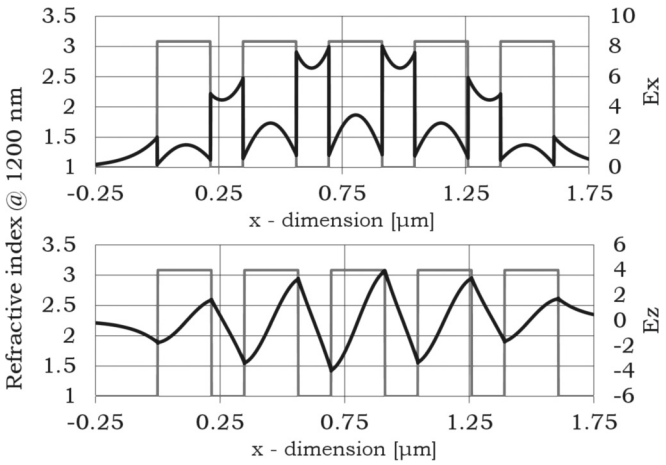

FIG. 6. Refractive index profile in an array of five GaP slab waveguides and corresponding electric field profiles E_x and E_z for the mode TM_0 at 1200 nm wavelength (pump wave).

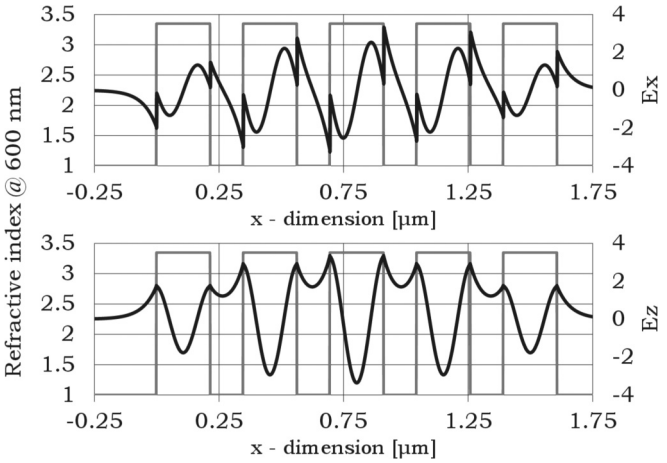

FIG. 7. Refractive index profile in an array of five GaP slab waveguides and corresponding electric field profiles E_x and E_z for the mode TM_1 at 600 nm wavelength (SHG wave).

not exactly the same as for the lowest modal phase mismatch. The discrepancy indicates that the field overlap, which is dependent on the wavelength, gives significant contribution to SHG process with respect to the modal phase-matching condition [Eqs. (3) and (4)]. Since the phase mismatch is proportional to the waveguide length, the above discrepancy vanishes for longer waveguides.

IV. FABRICATION AND CHARACTERIZATION OF THE NANOWAVEGUIDE ARRAYS

In this work, we used *e*-beam lithography (EBL) and dry etching to fabricate GaP NPs and SWs. Details of the fabrication process can be found in [20]. SiO_2 was used as the etch mask and was deposited on a double-side polished undoped [001] GaP substrate. This step was followed by spin

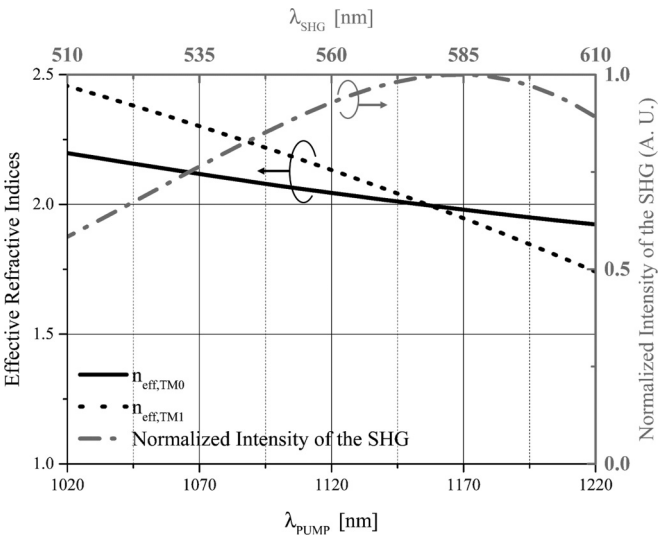

FIG. 8. Normalized intensity of the SHG light for an array of five GaP slabs (dashed-dotted line) and the effective refractive index of interacting modes in the SHG process: TM_0 of the pump (solid line), TM_1 of the SH light (dotted line).

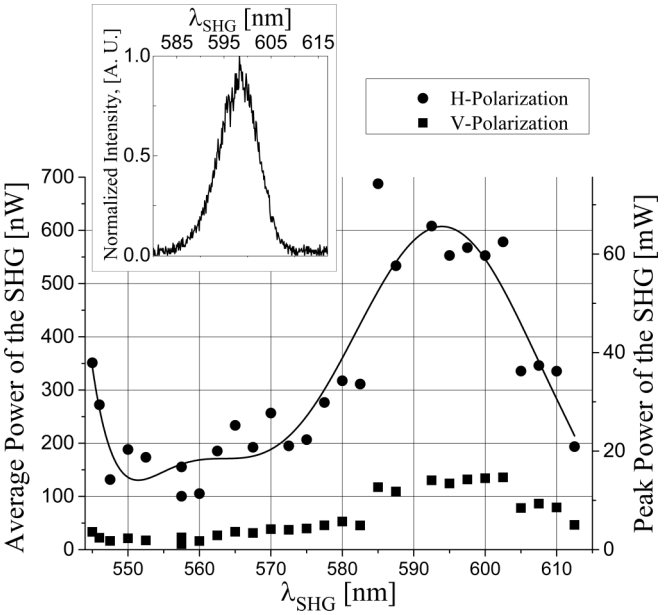

FIG. 9. Power of SHG light measured in an array of 5×5 GaP nanopillars. H and V polarization refers to the electric field polarization parallel and orthogonal to the pump, respectively. The solid line represents a fit to the experimental data. Left axis: measured average power. Right axis: corresponding peak power. Inset: example of a recorded spectrum for $\lambda_{pump} = 1195$ nm.

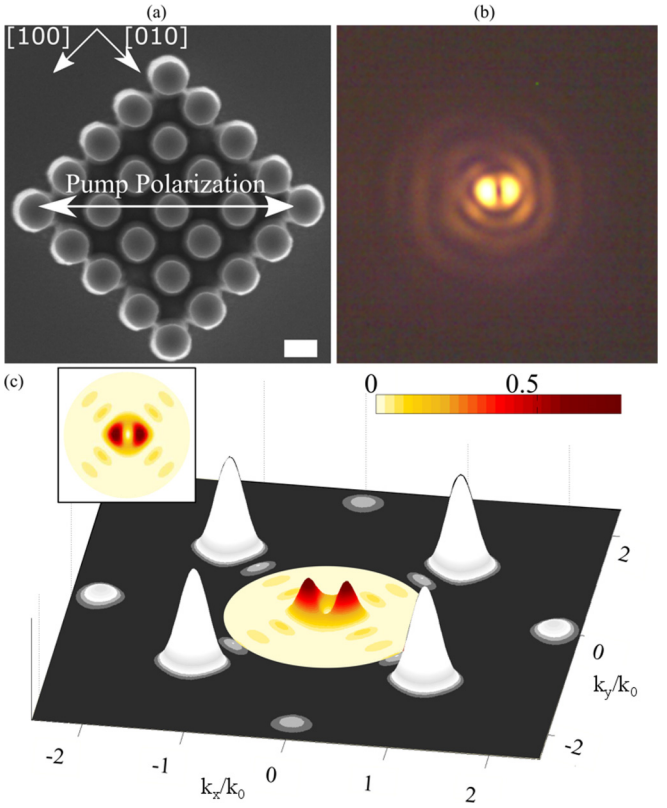

FIG. 10. Second-harmonic generation in an array of GaP nanopillars. (a) Top-view SEM image of the array of GaP nanopillars showing the orientation of the structure with respect to the crystallographic axes and the electric field polarization of the pump wave. The scale bar is 200 nm. (b) Second-harmonic generated light from an array imaged by CCD camera at $\lambda_{pump} = 1160$ nm. (c) Fourier decomposition of the intensity which results from superposition of the modes HE_{21} and TM_{01} at the end of the array of nanopillars. Inset: xy view.

coating of negative tone e-beam resist, and the structures were written by a Raith 150 EBL system. The pattern was transferred to the SiO_2 layer by reactive ion etching (RIE). We used inductively coupled plasma reactive ion etching (ICP-RIE) to transfer the pattern into GaP, using $Cl_2/H_2/CH_4$ chemistry. The residual masks were removed by buffered oxide etch (BOE).

For the array on NPs and the array of SWs the average dimensions are similar to the one presented in the simulation part (Sec. III). In particular, the length of the nanostructures fabricated is 750 nm. The reported values are averages due to the differences among the pillars/slab waveguides of the same array (approximately 10 nm) and the difference in radius/width between top and bottom surfaces (on the order of 100 nm).

In order to characterize the nanowaveguides, a Ti:sapphire pulsed laser (150 fs, 82 MHz repetition rate) with an optical parametric oscillator (OPO), ranging from 1090 to 1230 nm, was used. The pump beam with an average power density of 2.4 mW μm^{-2}, which corresponds to a pump peak power density of 20 GW cm^{-2}, was used to excite the fundamental mode of the structure. Additionally, a polarizer allowed to differentiate the electric field polarization of the collected light, parallel or orthogonal to the linearly polarized pump and identified with H or V, respectively. Finally, the SHG light was collected by an objective $50\times$, with NA $= 0.5$.

In Fig. 9, the power of the SHG light for an array of NPs as a function of the pump wavelength ranging from 1090 to 1230 nm is presented. The spectrum of the converted light was recorded for each pump wavelength, showing that the center of the detected light corresponded to $\lambda_{pump}/2$, which confirms the SHG process. An example of the recorded spectrum is presented in the inset in Fig. 9. The efficiency for the SHG process measured at the pump wavelength of 1190 nm was 10^{-4}, which corresponds to 50 W^{-1} cm^{-2}, after the normalization to the pump peak power on the surface of the array and the square of the length of the nanopillars.

For the fabrication of the array of NPs, we used a GaP wafer with (001) orientation; therefore, the substrate does not contribute to the detected SHG light. Here, the larger extinction ratio detected between H and V polarization confirms phase matching between the two second-order modes ($HE_{21} + TM_{01}$). The signal detected for the V polarization is not negligible because of the stronger contribution of TM_{01} coming from the enhancement caused by the nonlinear polarization density $P_z^{(2)}$. We attribute the difference in the SHG spectrum (Fig. 9) compared to the simulation (Fig. 5) to the slightly conical shape and different diameters of the NPs in the array, as well as the wavelength dependency of the nonlinear coefficient.

The pump polarization with respect to the structure and the wafer orientation is presented in Fig. 10(a). In Fig. 10(b) the far-field image of the SHG light from the array, recorded by the CCD camera, is presented for 1160 nm pump wavelength. In Fig. 10(c), the Fourier decomposition of the guided

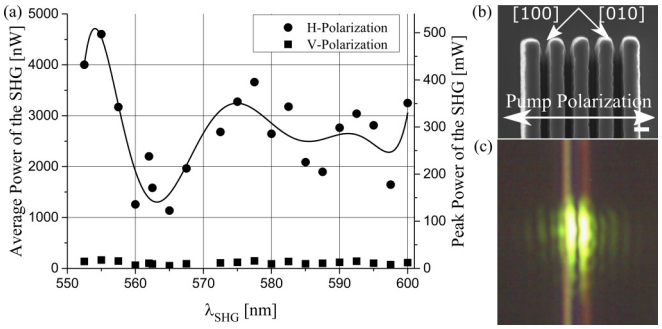

FIG. 11. Second-harmonic generation in an array of GaP slab waveguides. (a) Measured SHG light power in an array of five slab waveguides. H and V polarization refers to the electric field polarization parallel and orthogonal to the pump, respectively. The solid line represents a fit to the experimental data. Left axis: measured average power. Right axis: corresponding peak power. (b) Top-view SEM image of the array of GaP slab waveguides showing the orientation of the structure with respect to the crystallographic axes and the electric field polarization of the pump wave. The scale bar is 200 nm. (c) Second-harmonic generated light from an array imaged by CCD camera at $\lambda_{\text{pump}} = 1140$ nm.

second-harmonic light generated in the array of nanopillars is presented. The emitted light, limited by the numerical aperture of NA = 1, is highlighted in Fig. 10(c). This is in good agreement with the light detected through the CCD camera, presented in Fig. 10(b). Higher harmonics, which are visible on the graph for NA > 1, are not emitted from the array and, therefore, the far-field profile corresponds to the solution of a single nanopillar waveguide.

We should note that our conversion efficiency of 10^{-4} is comparable to low-loss dielectric nanoantennas, based on AlGaAs [35] and GaAs [31] (near-infrared), and GaP [21] (visible wavelengths) with SHG conversion efficiency of 8.5×10^{-5}, 2×10^{-5} and 10^{-6} using pump peak powers of 7, 3.4, and 200 GW cm^{-2}, respectively. However, in contrast to nanoantennas, which are designed for fixed dimensions, in our design the conversion efficiency is limited by the nanowaveguide length, which depends only on the fabrication technology.

If one considers the array of SWs, it is possible to identify a larger extinction ratio between the H and the V polarizations [Fig. 11(a)], due to the interaction of only TM_1 mode. The orientation of the pump polarization with respect to the array of SWs and the crystallographic axes is presented in Fig. 11(b). The presence of an intense second-order mode is visible in Fig. 11(c), where the two lobes of the mode TM_1 are distinguishable.

V. CONCLUSIONS

In conclusion, we propose a technique to generate second-harmonic light based on modal phase matching. In our experiments we utilized GaP nanowaveguides (nanopillars and slab waveguides, fabricated by top-down approach). In the fabricated array of 5×5 nanopillars, the maximum efficiency of 10^{-4} was measured, which corresponds to 50 W^{-1} cm^{-2}.

We should note, though, that our presented method is applicable to any material with $-43m$ crystal symmetry, as it was presented in the theory part (Sec. II). We also demonstrated that the longitudinal component of the nonlinear polarization density could be used to enhance the conversion efficiency. Our method, with respect to quasi-phase-matching technique for a single-slab waveguide, shows larger conversion efficiency, due to comparable overlap of the interacting fields in addition to the use of modal dispersion.

It is worth mentioning that quasi-phase matching by periodic modulation of the nonlinear coefficient in GaP is in its early stages due to technological difficulties. In the case of modal phase matching, the top-down approach used in the fabrication of the presented nanostructures shows an advantageous way to overcome the technological difficulties. Moreover, the selected approach allows the integration of the nanostructures in devices that are more complex.

For this reason, the presented method based on modal phase matching on nanostructures in a $-43m$ material as a nanoscopic light source can have a substantial interest in the future development of an integrated quantum photonics device. The proposed approach can be a valuable tool in the creation of a localized light source for imaging and nonlinear beam shaping.

ACKNOWLEDGMENTS

The work was performed within the Linné Center for Advanced Optics and Photonics (ADOPT). Financial support from the Swedish Research Council VR (Grants No. 349-2007-8664 and No. 621-2013-5811) is acknowledged. R.S. acknowledges financial support from the Swedish Research Council VR, for his international postdoctoral grant (Grant No. 4.3-2015-06446).

[1] Y. Nakayama, P. J. Pauzauskie, A. Radenovic, R. M. Onorato, R. J. Saykally, J. Liphardt, and P. Yang, Nature (London) **447**, 1098 (2007).

[2] C. W. Liu, S. J. Chang, C. H. Hsiao, R. J. Huang, Y. S. Lin, M. C. Su, P. H. Wang, and K. Y. Lo, IEEE Photonics Technol. Lett. **26**, 789 (2014).

[3] E. De Luca, R. Sanatinia, S. Anand, and M. Swillo, Opt. Mater. Express **6**, 587 (2016).

[4] R. Sanatinia, M. Swillo, and S. Anand, Nano Lett. **12**, 820 (2012).

[5] W. T. M. Irvine, K. Hennessy, and D. Bouwmeester, Phys. Rev. Lett. **96**, 057405 (2006).

[6] X. Wei, S. C. Hong, X. Zhuang, T. Goto, and Y. R. Shen, Phys. Rev. E **62**, 5160 (2000).

[7] M. Fiebig, V. V. Pavlov, and R. V. Pisarev, J. Opt. Soc. Am. B **22**, 96 (2005).

[8] P. Figliozzi, L. Sun, Y. Jiang, N. Matlis, B. Mattern, M. C. Downer, S. P. Withrow, C. W. White, W. L. Mochan, and B. S. Mendoza, Phys. Rev. Lett. **94**, 047401 (2005).

[9] S. N. Son, J. J. Song, J. U. Kang, and C. S. Kim, Sensors **11**, 6125 (2011).

[10] W. G. F. Ditcham, A. H. R. Al-Obaidi, D. McStay, T. T. Mottram, J. Brownlie, and I. Thompson, Biosens. Bioelectron. **16**, 221 (2001).

[11] K. M. Yoo, Q. Xing, and R. R. Alfano, Opt. Lett. **16**, 1019 (1991).

[12] M. Han, G. Giese, and J. F. Bille, Opt. Express **13**, 5791 (2005).

[13] L. Moreaux, O. Sandre, and J. Mertz, J. Opt. Soc. Am. B **17**, 1685 (2000).

[14] S. J. Lin, R. J. Wu, H. Y. Tan, W. Lo, W. C. Lin, T. H. Young, C. J. Hsu, J. S. Chen, S. H. Jee, and C. Y. Dong, Opt. Lett. **30**, 2275 (2005).

[15] S. Brasselet, V. Le Floch, F. Treussart, J.-F. Roch, J. Zyss, E. Botzung-Appert, and A. Ibanez, Phys. Rev. Lett. **92**, 207401 (2004).

[16] S. Chen, W. Li, J. Wu, Q. Jiang, M. Tang, S. Shutts, S. N. Elliott, A. Sobiesierski, A. J. Seeds, I. Ross, P. M. Smowton, and H. Liu, Nat. Photonics **10**, 307 (2016).

[17] C. P. Dietrich, A. Fiore, M. G. Thompson, M. Kamp, and S. Höfling, Laser Photon. Rev. **10**, 870 (2016).

[18] V. L. Tassev, S. R. Vangala, R. D. Peterson, M. M. Kimani, M. Snure, R. W. Stites, S. Guha, J. E. Slagle, T. R. Ensley, A. A. Syed, and I. V. Markov, Opt. Mater. Express **6**, 1724 (2016).

[19] P. Guillemé, M. Vallet, J. Stodolna, A. Ponchet, C. Cornet, A. Létoublon, P. Féron, O. Durand, Y. Léger, and Y. Dumeige, Opt. Express **24**, 14608 (2016).

[20] R. Sanatinia, S. Anand, and M. Swillo, Nano Lett. **14**, 5376 (2014).

[21] J. Cambiasso, G. Grinblat, Y. Li, A. Rakovich, E. Cortés, and S. A. Maier, Nano Lett. **17**, 1219 (2017).

[22] P. S. Kuo, W. Fang, and G. S. Solomon, Opt. Lett. **34**, 3580 (2009).

[23] V. V. Pavlov, A. M. Kalashnikova, R. V. Pisarev, I. Sanger, D. R. Yakovlev, and M. Bayer, Phys. Rev. Lett. **94**, 157404 (2005).

[24] S. Buckley, M. Radulaski, K. Biermann, and J. Vučković, Appl. Phys. Lett. **103**, 211117 (2013).

[25] K. Moutzouris, S. Venugopal Rao, M. Ebrahimzadeh, A. De Rossi, M. Calligaro, V. Ortiz, and V. Berger, Appl. Phys. Lett. **83**, 620 (2003).

[26] D. C. Hutchings, S. J. Wagner, B. M. Holmes, U. Younis, A. S. Helmy, and J. S. Aitchison, Opt. Lett. **35**, 1299 (2010).

[27] S. J. Wagner, B. M. Holmes, U. Younis, I. Sigal, A. S. Helmy, J. S. Aitchison, and D. C. Hutchings, IEEE J. Quantum Electron. **47**, 834 (2011).

[28] A. M. Malvezzi, G. Vecchi, M. Patrini, G. Guizzetti, L. C. Andreani, F. Romanato, L. Businaro, E. Di Fabrizio, A. Passaseo, and M. De Vittorio, Phys. Rev. B **68**, 161306 (2003).

[29] S. Ducci, L. Lanco, V. Berger, A. De Rossi, V. Ortiz, and M. Calligaro, Appl. Phys. Lett. **84**, 2974 (2004).

[30] A. Fiore, S. Janz, L. Delobel, P. van der Meer, P. Bravetti, V. Berger, E. Rosencher, and J. Nagle, Appl. Phys. Lett. **72**, 2942 (1998).

[31] S. Liu, M. B. Sinclair, S. Saravi, G. A. Keeler, Y. Yang, J. Reno, G. M. Peake, F. Setzpfandt, I. Staude, T. Pertsch, and I. Brener, Nano Lett. **16**, 5426 (2016).

[32] X. Yu, L. Scaccabarozzi, J. S. Harris Jr, P. S. Kuo, and M. M. Fejer, Opt. Express **13**, 10742 (2005).

[33] F. M. Pigozzo, D. Modotto, and S. Wabnitz, Opt. Lett. **37**, 2244 (2012).

[34] D. Duchesne, K. A. Rutkowska, M. Volatier, F. Légaré, S. Delprat, M. Chaker, D. Modotto, A. Locatelli, C. De Angelis, M. Sorel, D. N. Christodoulides *et al.*, Opt. Express **19**, 12408 (2011).

[35] R. Camacho-Morales, M. Rahmani, S. Kruk, L. Wang, L. Xu, D. A. Smirnova, A. S. Solntsev, A. Miroshnichenko, H. H. Tan, F. Karouta *et al.*, Nano Lett. **16**, 7191 (2016).

[36] D. E. Aspnes and A. A. Studna, Phys. Rev. B **27**, 985 (1983).

[37] I. Shoji, T. Kondo, A. Kitamoto, M. Shirane, and R. Ito, J. Opt. Soc. Am. B **14**, 2268 (1997).

[38] D. L. Perry, *Handbook of Inorganic Compounds*, 2nd ed. (CRC Press, Boca Raton, FL, 2016), p. 184.

[39] V. Berger, Phys. Rev. Lett. **81**, 4136 (1998).

[40] S. Keren-Zur, O. Avayu, L. Michaeli, and T. Ellenbogen, ACS Photonics **3**, 117 (2016).

[41] A. Arbabi, Y. Horie, M. Bagheri, and A. Faraon, Nat. Nanotechnol. **10**, 937 (2015).

[42] M. Khorasaninejad, W. T. Chen, R. C. Devlin, J. Oh, A. Y. Zhu, and F. Capasso, Science **352**, 1190 (2016).

[43] A. Yariv and P. Yeh, *Photonics: Optical Electronics in Modern Communications*, 6th ed., The Oxford Series in Electrical and Computer Engineering (Oxford University Press, Oxford, 2007), p. 363.

[44] H. Kogelnik, Theory of dielectric waveguides, in *Integrated Optics*, edited by T. Tamir (Springer, Berlin, 1975), pp. 13–81.

[45] J. L. P. Hughes and J. E. Sipe, Phys. Rev. B **53**, 10751 (1996).